CrossMark

Optical and photo catalytic characteristics of Ag_2S/TiO_2 nanocomposite films prepared by electrochemical anodizing and SILAR approach

M. M. Momeni[1] · Y. Ghayeb[1] · A. A. Mozafari[1]

Abstract Ag_2S decorated titanium oxide nanotubes (Ag_2S/NTs) were prepared by electrochemical anodizing and successive ionic layer adsorption and reaction (SILAR) approach. The prepared samples were characterized by X-ray diffraction, field emission scanning electron microscopy coupled with energy dispersive X-ray analysis and diffuse reflectance spectroscopy. SEM results indicate titanium oxide nanotubes (NTs) with 90–220 nm in diameter and 15–30 nm in wall thickness were prepared by one-step anodizing method on the surface of titanium foils. Characterization of the Ag_2S/NTs samples indicated that the number of SILAR cycles influenced the morphology of fabricated films. The degradation of rhodamine B was used as a model reaction to evaluate the photo catalytic activity of the obtained samples. Results showed that the photo catalytic activity of Ag_2S/NTs nanocomposite samples is higher than that with bare NTs sample. The incorporation of Ag_2S on NTs improves the photo catalytic activity due to the synergetic effect. Ag_2S/NTs nanocomposite sample prepared by SILAR deposition with 2 cycles gives the highest degrading rate, which can be attributed to appropriate Ag_2S content and high surface area of this sample. Ag_2S/NTs nanocomposites are easy to be recycled and have good stability for repeated use. With the improved visible light degradation performance, Ag_2S/NTs samples would be expected to be used in water purification. Since these prepared electrodes can be easily removed and replaced after the photo catalytic reaction, avoiding the filtration step after photoreaction or the immobilizing

process required for photo catalyst particles, the operation in the photo-reactor becomes much easier from an engineering point of view.

1 Introduction

Nowadays, semiconductor photo catalysts have been attracted widely attention since the environment pollution problem becomes seriously [1–4]. As a kind of semiconductor, titanium dioxide (TiO_2) was recognized as the best photo catalyst to decompose the organic compounds for the treatment of waste water and air pollution due to its outstanding performance, such as broad functionality, long-term stability, low energy consumption and non-toxicity [5–8]. The nanoscale TiO_2, especially the TiO_2 nanotube has better photo catalytic activity than TiO_2 powders because of its unique structural and electronic properties [9–12]. Self-ordering titanium oxide nanotubes synthesized by anodization process have been of a great significance in the field of solar cells, gas sensors, photo-catalysis, biomedical implants, water splitting and batteries [11–13]. However, the problem is that the band edge of TiO_2 photo catalyst lies in the UV region which covers about 4 % of the solar spectrum [12, 13]. Consequently conventional TiO_2 photo catalysts are inactive under visible-light irradiation and as a result with limited practical applications. In order to solve this problem, the titanium dioxide is usually modified using various methods. One of the ways to do this is to combine TiO_2 with another semiconductor with narrow band gap (sensitization) such as CdS, CdSe, PbS, PbSe, Ag_2S and CdTe. Compared to other sensitizers, semiconductors have unique advantages. The band gap of semiconductors can be easily tuned by varying the particle size. Another important advantage of semiconductor

✉ M. M. Momeni
 m_m_momeny22@yahoo.com

1 Department of Chemistry, Isfahan University of Technology, Isfahan 84156-83111, Iran

 Springer

nanoparticles is their use in photo catalysis [14–19]. Among the low band gap semiconductors, silver sulfide (Ag_2S) has attracted much attention; it could absorb intense visible light and attractive interest. Ag_2S is a good candidate for the photosensitization of TiO_2 and it is a direct band gap semiconductor with a low band gap ($\sim$0.9–1.1 eV). It is a promising material which responds in the whole solar energy spectrum. Moreover, the conduction band of Ag_2S is less anodic (-0.3 eV) than that of TiO_2 (-0.1 eV). The valence band of Ag_2S is more cathodic ($+0.7$ eV) than that of TiO_2 ($+3.1$ eV) and it has a large absorption coefficient in the visible region [19–24]. Although there were some reports about the coupling of TiO_2 with Ag_2S semiconductor, rarely studies regarding titanium oxide nanotubes and Ag_2S were conducted [25, 26]. Moreover, the previous fabrication strategies were mainly focused on the hydrothermal process and source decomposition method, in which harsh conditions and expensive apparatus were necessary. Therefore, in this study, titanium oxide nanotubes (TNs) were firstly fabricated by anodization of titanium substrate. Subsequently, As_2S decorated titanium oxide nanotubes (Ag_2S/NTs) were constructed through successive ionic layer adsorption and reaction (SILAR) strategy. The resulting samples were characterized by scanning electron microscopy (SEM), X-ray diffraction (XRD), and Ultraviolet–visible diffuse reflectance spectra (UV–Vis DRS). In addition, photo catalytic activity of hybrid silver sulfide-titanium oxide nanostructures was investigated and compared by degradation of some dyes. Results show that the presence of silver sulfide significantly improved the photo catalytic performance of samples.

2 Experimental

All chemicals were obtained as analytical reagent grade and used without further purification. The solutions were prepared with distilled water. Titanium foils (purity >99.99 %, 1 mm thickness) were used.

Titanium plates were cut into desired dimensions and were employed as substrate for the preparation of the TNs/Ti working electrode with only one face exposed to solution. They were mechanically polished with different abrasive papers (with the following grades: 80,180, 400, 600, 1200 and 2000), rinsed in a bath of distilled water, then chemically etched by immersion in a $HF/HNO_3/H_2O$ (1:4:5 in volume) mixed solution, and finally rinsed with distilled water. They were then dried in air at room temperature. Pretreatment by this procedure ensures a good adhesion of the deposit to the substrate. After cleaning, anodic films were grown from titanium by anodizing of this

foil in a solution of ethylene glycol (98 mL) containing 0.13 M NH_4F and 2 mL distilled water at a constant voltage of 60 V for 6 h at room temperature using a graphite foil with about 12 cm^2 geometric areas as cathode. Anodizing was carried out using a controlled DC power supply source (ADAK, PS405). After anodizing, the as-formed samples were annealed in air atmosphere at 400 °C for 2 h with a ramp of 2 °C/min to obtain crystalline samples.

Silver sulfide (Ag_2S) was deposited on TNs by separately SILAR method. TNs were dipped into 0.1 M $AgNO_3$ in ethanol for 1 min, rinsed with ethanol and dipped for 3 min into a 0.1 M Na_2S methanol solution and rinsed again with ethanol, which was defined as one SILAR cycle. The deposition of Ag_2S was repeated for 8 cycles. In order to investigate the influence of deposition conditions on samples property, we changed the deposition cycle (0, 2, 3, 4, 5, 6 and 8 cycles) into carry out the Ag_2S/NTs samples. The as prepared samples were named respectively S0, S2, S3, S4, S5, S6, and S8, that terminal number is the number of SILAR cycles. A schematic representation of the anodizing setup and producing process of NTs films on titanium and deposition of Ag_2S on these films by SILAR method is presented in Fig. 1.

The surface morphology of all samples was characterized by field emission scanning electron microscopy (FE-SEM, Hitachi S-4160, Japan), and the elemental composition was estimated by energy dispersive X-ray spectroscopy (EDX). Elemental mapping was conducted by energy dispersive spectroscopy (EDS). The crystalline phases were identified by XRD (Philips ́XPert). Diffraction patterns were recorded in the 2θ range from 20° to 80° at room temperature. The optical absorption of the samples were determined using a diffuse reflectance UV–visible spectrophotometer (JASCO V-570).

Photo catalytic activity tests using the Ag_2S/NTs nanocomposites were performed at room temperature. The photo catalytic reaction was carried in a single-compartment cylindrical quartz reactor. A 200 W xenon lamp accompanied with a UV cutoff filter was used as a light source to provide visible light. The luminous intensity of the xenon lamp was 100 mW cm^{-2}. Prior to illumination, the photo catalyst sample was immersed in quartz reactor containing rhodamine B, magnetically stirred for 90 min in the dark in order to reach adsorption–desorption equilibrium. Then the solution was irradiated in visible light irradiation under magnetic stirring for various time intervals (5–90 min). After periodic time intervals, specific amount of the solution was withdrawn and the changes in concentration of rhodamine B were analyzed by monitoring the absorbance at 554 nm using a UV–Vis spectrophotometer.

Fig. 1 Schematic presentation of producing process of NTs nanotube films on titanium foils and deposition of Ag$_2$S on these films by SILAR method
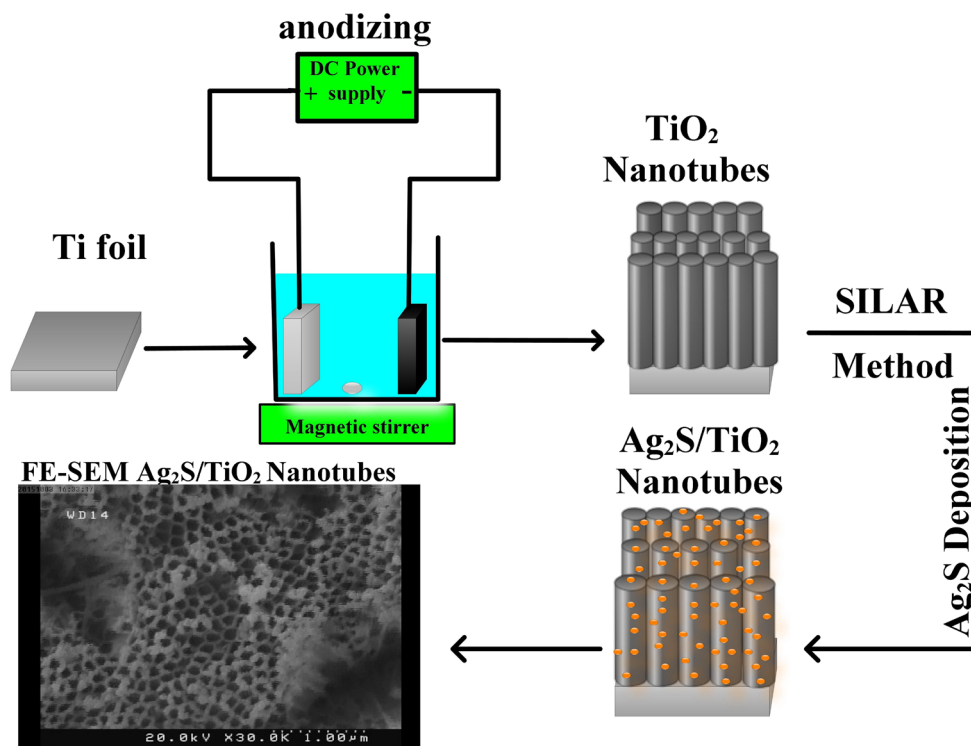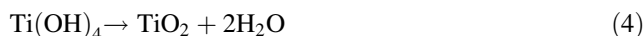

3 Results and discussion

Anodizing is an electrolytic passivation process used to increase the thickness of the natural oxide layer on the surface of metal parts. The process is called anodizing because the part to be treated forms the anode electrode of an electrical circuit. The anodized titanium layer is grown by passing a direct current through an electrolytic solution, with the titanium object serving as the anode (the positive electrode). The current releases hydrogen at the cathode (the negative electrode). Alternating current and pulsed current is also possible but rarely used. The voltage required by different solutions is variable. Higher voltages are typically required for thicker coatings formed in organic solution. The anodizing current varies with the area of titanium being anodized. Titanium anodizing is usually performed in an organic solution which slowly dissolves the titanium oxide. Conditions such as electrolyte concentration, acidity, solution temperature, and current must be controlled to allow the formation of a consistent oxide layer. Anodizing is an electrolytic process that creates a protective or decorative oxide film over a metallic surface. In anodizing of titanium, the outer anodic layer (partly exposed to the electrolyte) has an excess of hydroxyl ions compared to the inner layer and is considered to be Ti(OH)$_4$. The inner layer, where the de-hydroxylation of the film (water releasing) has occurred, is represented as TiO$_2$. In reality there is likely to be a concentration gradient across the film, which can be written as TiO$_2$·xH$_2$O, to represent the inner (dry) and outer (hydrated) anodic oxide. The reactions which occur at the anode are:

- Oxidation of the metal which releases Ti^{4+} ions and electrons, Eq. (1):

$$2Ti \rightarrow 2Ti^{4+} + 8e^- \tag{1}$$

- Combination of Ti^{4+}ions with OH$^-$ and O^{2-} species provided by the water.

Equations (2) and (3) below account for the hydrated anodic layer and the oxide layer. Further oxide is produced when the hydrated anodic layer releases water by a condensation reaction, Eq. (4):
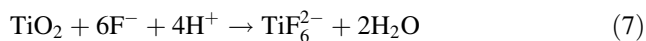
$$Ti^{4+} + 4OH^- \rightarrow Ti(OH)_4 \tag{2}$$

$$Ti^{4+} + 2O_2^{2-} \rightarrow TiO_2 \tag{3}$$

$$Ti(OH)_4 \rightarrow TiO_2 + 2H_2O \tag{4}$$

At the cathode there is hydrogen evolution, Eq. (5):

$$8H^+ + 8e^- \rightarrow 4H_2 \tag{5}$$

By summing the equations from (1) to (5), the overall process of oxide formation is given:

$$Ti + 2H_2O \rightarrow TiO_2 + 2H_2 \tag{6}$$

Furthermore, the fluorine ions can attack the hydrated layer and the oxide, as described in the Eqs. (7) and (8), or react with Ti^{4+}, Eq. (9), the ions being mobile in the anodic layer, under the high applied electric field:

$$TiO_2 + 6F^- + 4H^+ \rightarrow TiF_6^{2-} + 2H_2O \qquad (7)$$

$$Ti(OH)_4 + 6F^- \rightarrow TiF_6^{2-} + 4OH^- \qquad (8)$$

$$Ti^{4+} + 6F^- \rightarrow TiF_6^{2-} \qquad (9)$$

Clearly, the competition between formation of the oxide (see Eqs. (2)–(4)) and its dissolution (see Eqs. (7)–(9)), is the key factor in determining the anodic titanium oxide structure produced [27].

The SILAR technique is a solution phase method to grow thin films at room temperature and ambient pressure. In the SILAR technique, the cation and anion constituents of thin film material are adsorbed on the surface of the substrate one at a time from different precursor solutions. Between each precursor treatment, the surface is rinsed with purified solvent, so that only the tightly adsorbed layer stays on the substrate. Hence, the reaction producing a thin film occurs only on the surface of the substrate. In SILAR method, the growth mechanism involves three most important steps:

1. Specific adsorption of the most strongly adsorbed ions of the compound to be grown by substrate immersion in a solution of one of its salts
2. Water or ethanol rinsing of the excess solution still adhering to the substrate
3. Chemical reaction between the most strongly specifically adsorbed ions and the less strongly adsorbed ones by the subsequent substrate immersion in a solution containing the latter, entailing the growth [28].

The morphology of Ag_2S/NTs nanocomposite samples were observed by SEM. Figure 2a shows FE-SEM images of S2 sample, which clearly shows existence of decorated nanotubes on the surface of titanium that the surface of them was open. It can be seen that after decoration with Ag_2S, the nanotubular architecture could still be observed without significantly morphological transformation. In addition, numerous Ag_2S aggregation was irregularly covered onto the surface of TiO_2 nanotubes. S2 sample were still with high orientation and open top characteristics without losing their architectures, which was essential to a high photo catalytic activity. By increasing the cycle number of SILAR, more amounts of Ag_2S have been deposited on the surface. In S3 sample (Fig. 2b), nanostructure films can not be seen on the surface. Compact films, without porosity, were formed on the surface of samples. It can be said that when the number of SILAR

cycles increased to 2 cycles, surface is covered with a compact layer of silver sulfide.

The analysis of the films surface by energy dispersive X-ray spectroscopy (EDX) taking measurements on top and results present in Fig. 3. It was seen that the films mainly consisted of Ti, O, Ag and S; the contents of each sample were inserted in the corresponding figure. The EDX data of Ag_2S/NTs nanocomposite samples show two peaks around 4.5 and 4.9 keV for Ti. The peaks due to silver are clearly distinct at 2.9 and 3.1 keV. Also peaks due to sulfur were appeared at 0.1 and 2.3 keV. These results confirm that Ti, O, Ag and S exist in these samples. The occurrences of traces of contaminants such as N, F and Na from precursors are also observed. The composition of the Ag_2S/NTs nanocomposite sample was confirmed by energy-dispersive X-ray mapping (Fig. 4). This test shows the presence of Ag, O, Ti, S, Na, F and N in these samples. The elemental maps demonstrated that Ag, Ti, O and S are homogeneously distributed on the surface of samples.

The phase structures of samples were determined by X-ray diffraction (XRD). The XRD patterns of the bare TiO_2 and Ag_2S/NTs samples are shown in Fig. 5. Figure 5 shows XRD patterns of (a) as-prepared bare TiO_2, (b) bare TiO_2 annealed at 400 °C and (c) Ag_2S/NTs samples. Diffractions that are attributable to anatase TiO_2 are clearly observed in the annealed sample. The Ti peaks were due to the titanium substrate. As shown in this figure, the peaks at $2\theta = 25.4°, 37.0°, 37.9°, 38.6°, 48.2°, 54.0°, 55.2°, 62.9°, 68.9°, 75.3°$ and $76.2°$ were assigned to the TiO_2 anatase phase (JCPD card no. 01-073-1764). Comparing the XRD patterns of b and c show that apart from the existed diffraction peaks in b and c spectra which are related with the characteristic diffraction peaks of TiO_2, other specific diffraction peaks at $28.9°, 31.5°, 43.4°, 45.4°, 46.3°, 48.7°$ and $50.2°$ also appear in c spectrum. According to the standard PDF (JCPD card no. 00-014-0072) of Ag_2S, the seven extra specific diffraction peaks in c spectrum correspond with (111), (−112), (200), (−113), (−123), (014) and (−114) of crystal planes of silver sulfide. The XRD data further confirms the successful preparation of Ag_2S/NTs photo catalysts.

Diffuse reflectance spectral analysis in the UV–visible region was carried out for pure Ag_2S, bare TiO_2 and all the Ag_2S/NTs nanocomposites (S1–S8). UV–Vis diffuse reflectance spectra of pure Ag_2S were recorded to analyze the influence of Ag_2S on the absorption of Ag_2S/NTs nanocomposites. The Ag_2S with a narrow band gap display a significant growth trend with the increase of the wavelength in the range of 400–600 nm (Fig. 6a). The band gap of Ag_2S was determined by extrapolating the function of $(\alpha h\upsilon)^2$ in term of $h\upsilon$ as shown in the Fig. 6a and it was found that the band gap of Ag_2S is around 1.1 eV, which is in good agreement with previous reports for the band gap
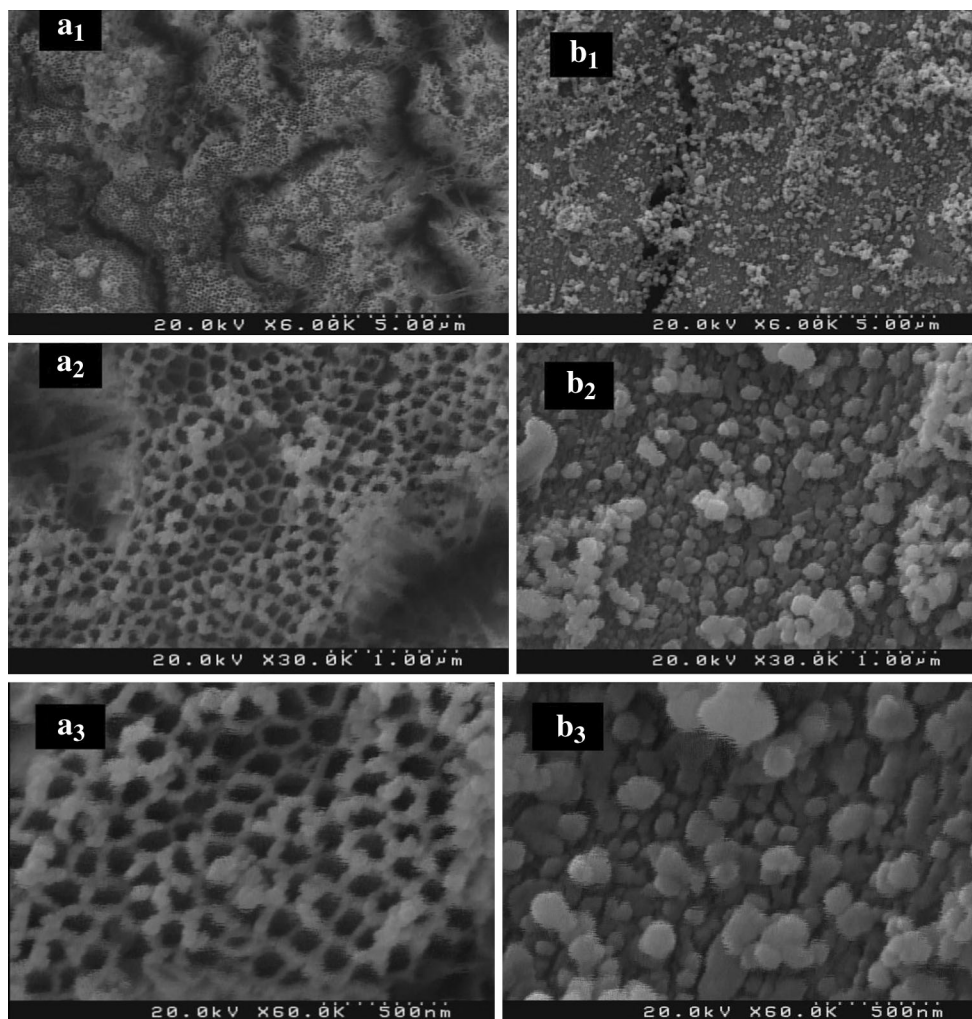
Fig. 2 SEM *top-view* image of different samples; **a** S2 and **b** S3

energy of Ag_2S nanoparticles (0.9–1.1 eV) [29, 30]. Figure 6b recorded the typical UV–Vis DRS spectrum of different samples prepared with different cycles of SILAR processes. Meanwhile, pristine TiO_2 sample was measured as the reference. Clearly, as shown in Fig. 6b, TiO_2 performed typical absorbance with an intense transition in the UV region of the spectra, corresponding the electronic transition from O^{2-} anti-bonding orbital to the lowest empty orbital of Ti^{4+} ($O2p \rightarrow Ti3d$). Compared with the pristine TiO_2, it can be obviously observed that the light absorbance edge of Ag_2S/NTs nanocomposites was red-shifted to visible region ranging from 400 to 600 nm, and the wide visible-light absorption becomes stronger with increasing Ag_2S content.

Photo catalytic activity of different samples was followed through degradation of Rhodamine B as a function of irradiation time with visible light. To get the response of photo catalytic activities of bare TiO_2 and Ag_2S/NTs nanocomposites, the absorption spectra of exposed samples

at various time intervals were recorded and the rate of color degradation was observed in terms of change in intensity at λ_{max} of these dyes. In practice, the first, dyes degradation experiments were conducted under light irradiation to evaluate direct photolysis without the addition of any catalyst. The concentration of dyes remained nearly constant after irradiation. Thus, no obvious degradation of these dyes was observed in this time period. In addition, a dark control experiment was conducted, indicating that the adsorption of these dyes onto the surface of the catalyst in the absence of light radiation was negligible. The photo catalysis results indicated that the photo catalytic process was very effective in the removal of these dyes and it was observed that the degradation of dyes was enhanced using Ag_2S/NTs samples. Figure 7a shows the photo degradation rate of Rh B under visible light in presence of different samples. Under the irradiation of visible light, bare TiO_2 sample showed almost no photo catalytic activity, but Ag_2S/NTs samples showed photo catalytic activity.
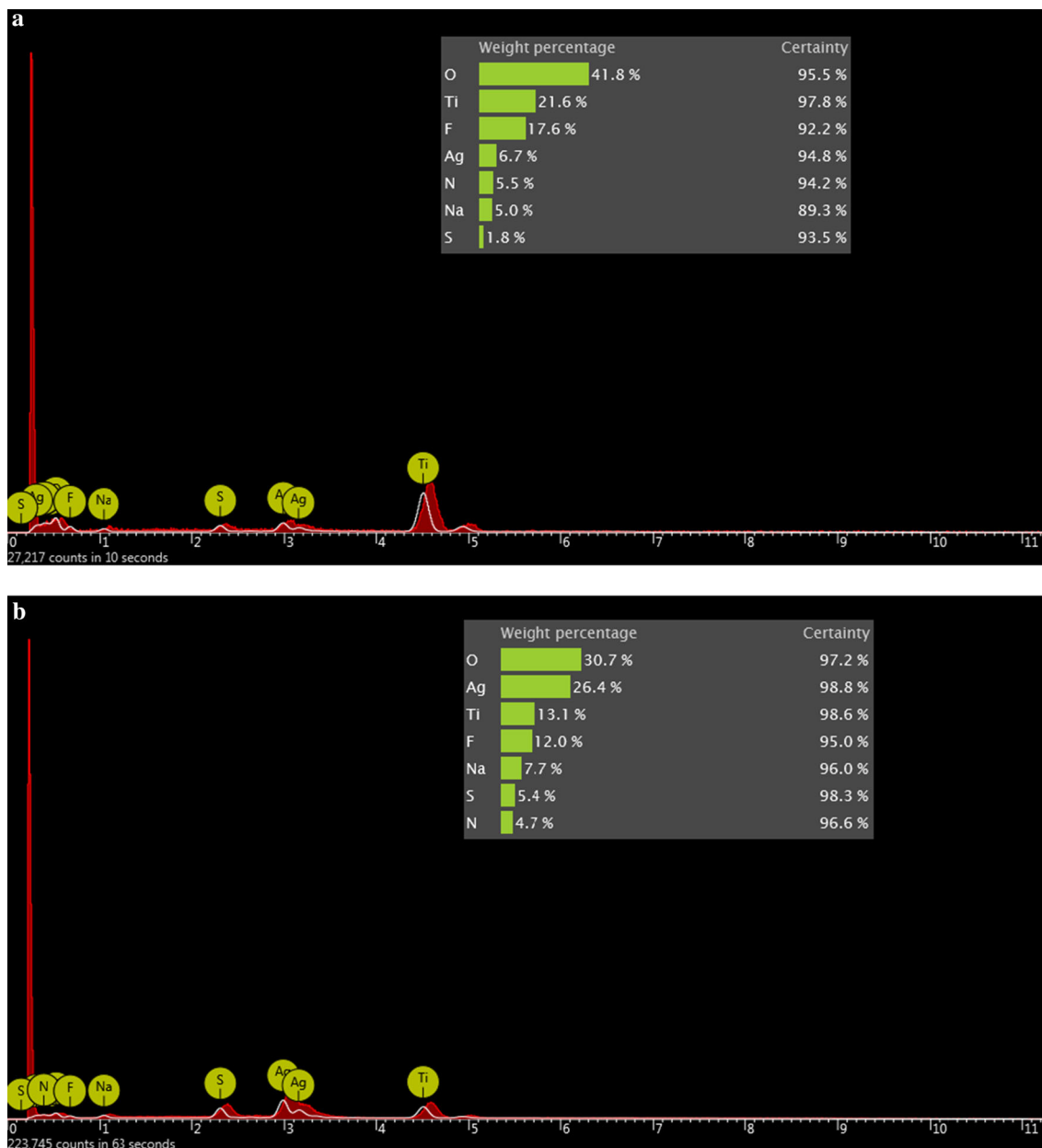
Fig. 3 EDX spectrum of different samples; **a** S2 and **b** S8 sample

Figure 7a show that the S2 sample exhibited better photo catalytic activity than other samples under visible light illumination. The photo catalytic performances of different samples were in the following order:

S2 > S3 > S4 > S5 > S8 > S6 > S0

For estimating quantitatively photo catalytic activities of the different samples, the pseudo-first order reaction is employed to calculate the rate constant (k) of Rh B degradation. The ratio of absorbance A_t of Rh B at time t to A_0 measured at t = 0 must be equal to the concentration ratio C_t/C_0 of Rh B. The kinetic equation for the reduction can be written as [31–33]

$$\ln(A_t/A_0) = \ln(C_t/C_0) = -kt \tag{10}$$

Its $\ln(C_t/C_0)$ plot shows a linear relationship with the irradiation time. The observed linearity in the plot of $\ln(C_t/C_0)$ versus irradiation time (Fig. 7b) signifies that the degradation of the test dye follows pseudo first-order kinetics, represented by the equation. The calculated rate constants and correlation coefficients corresponding to Fig. 7b are listed in Table 1.
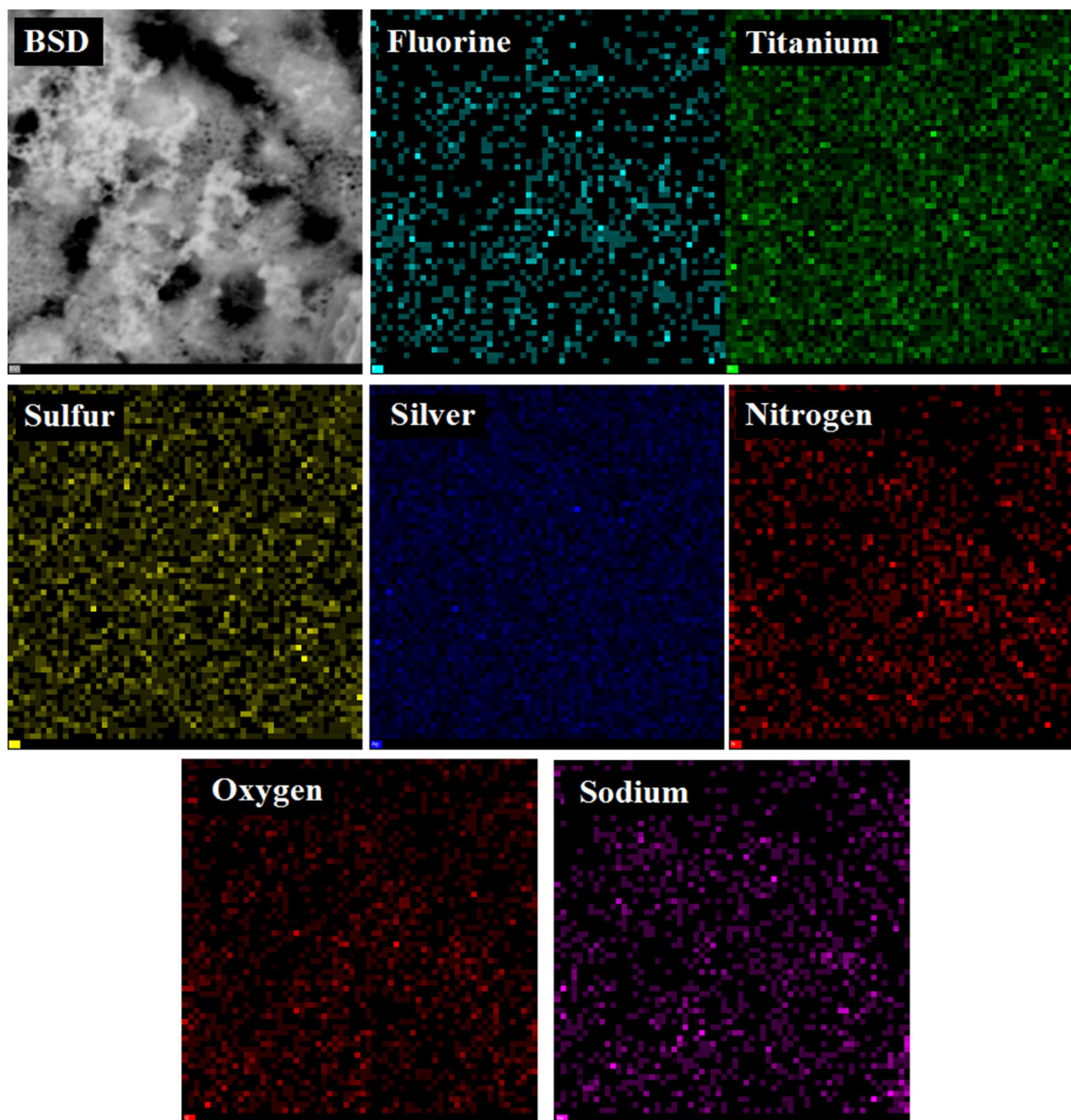
Fig. 4 Elemental EDX mapping of Ti, O, Ag and S obtained from S8 sample

In addition to the photo catalytic activity, the stability of the photo catalysts is another important issue for practical application, for it can be regenerated and reused. To investigate the stability of prepared sample, six runs of cycling photo degradation experiments under identical conditions were performed (Fig. 7c). Before each experiment, the used photo catalyst was cleaned through washing with distilled water. Compared with the common catalysts in the powder form that nanoparticles dispersed in the reaction media, our samples prepared on the titanium substrates are more conveniently separated and recycled without any laborious centrifugation. As shown in Fig. 7c, after a 6-cycle experiment, this catalyst exhibited similar catalytic performance without significant deactivation,

indicating its high durability and stability. Therefore, the recycling of S2 is possible, prepared samples in this study should be a promising photo catalyst for treatment of organic contamination.

In here, a simple photo catalytic mechanism has been investigated. Figure 8 shows the schematic diagram of the separation of photo-generated electrons-holes pairs on the interface of Ag_2S/NTs under visible light irradiation. When the Ag_2S/NTs nanocomposites were irradiated by the visible light, electrons from the valence band (VB) of Ag_2S (due to its narrow energy band gap that is ~ 1 eV) get excited to its conduction band (CB) with simultaneous generation of the same amount of holes in its VB [Reaction (11)]. Then, the photo-induced electrons and holes could be
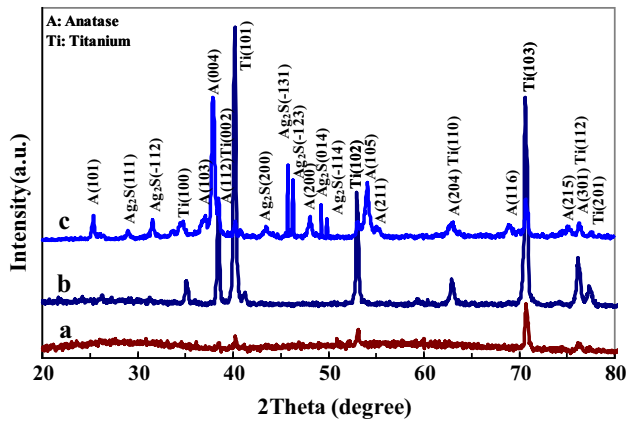
Fig. 5 XRD patterns of prepared samples *a* as-prepared bare TiO$_2$, *b* bare TiO$_2$ annealed at 400 °C for 2 h and *c* S8 sample
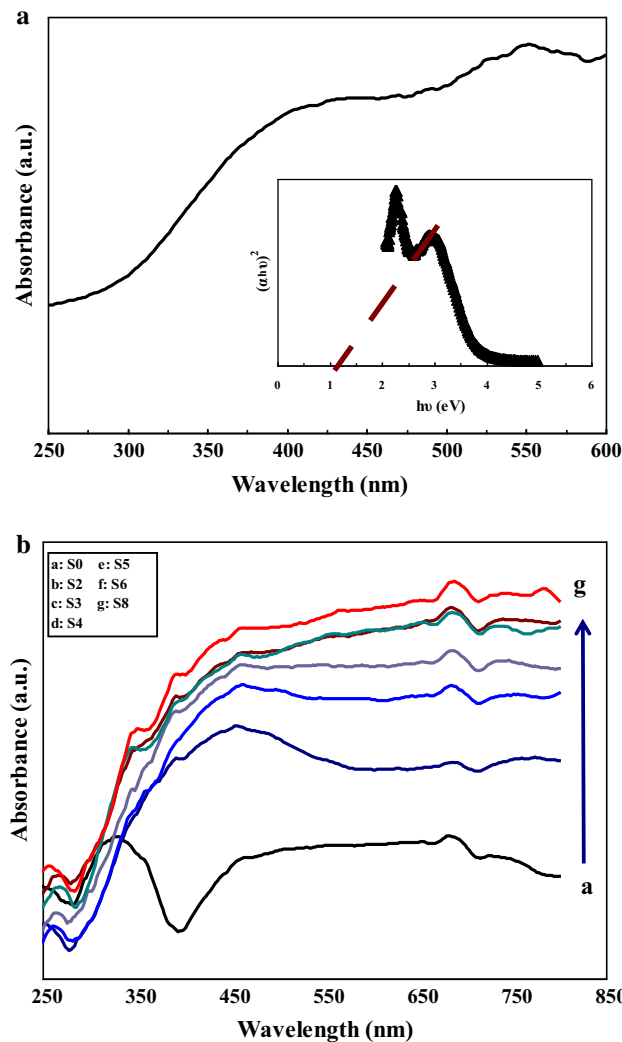

Fig. 6 a UV–Vis reflectance spectrum of Ag$_2$S sample; *Inset* $(\alpha h\upsilon)^2$ versus hυ for Ag$_2$S. **b** Diffuse reflectance UV–Vis absorption spectra of different samples
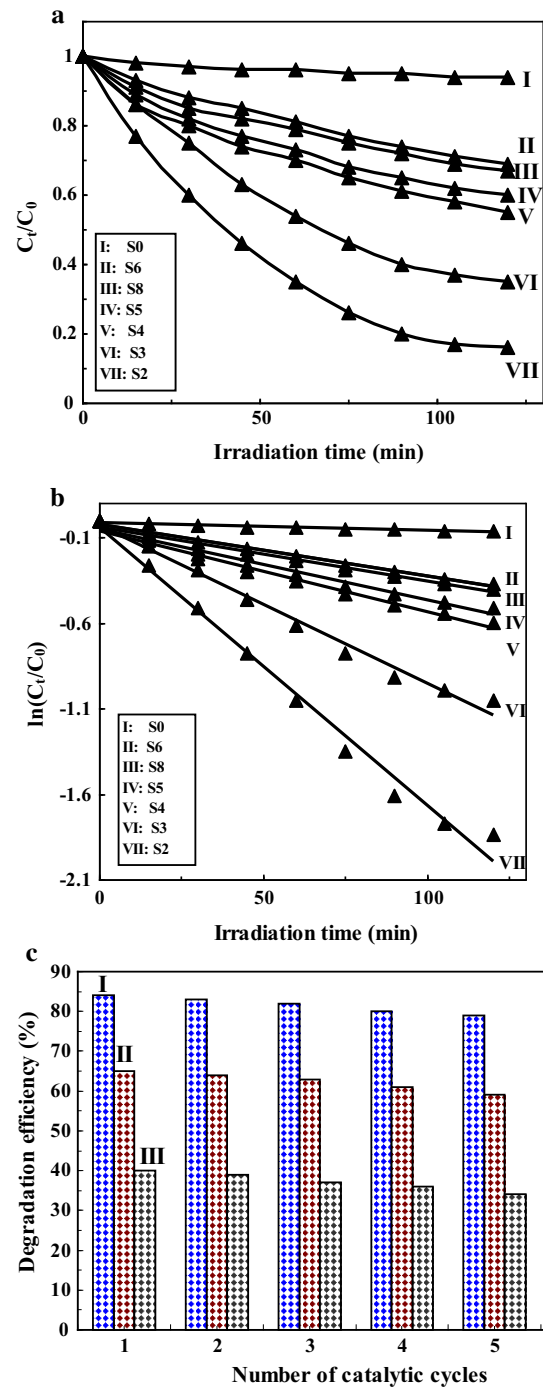

Fig. 7 a The photo catalytic degradation of Rh B solution over the different samples under visible light irradiation. **b** Ln(C$_t$/C$_0$) versus irradiation time plot. **c** Photo catalyst stability test of prepared samples

separated under the influence of the electrostatic field induced by the different work functions of the semiconductors their VB [34]. Since the conduction band of TiO$_2$ is more positive than that of Ag$_2$S, electrons from the conduction band of Ag$_2$S get transferred to the conduction

Table 1 The apparent first-order rate constant (k) of photo catalytic degradation of Rh B for different samples

Samples	Apparent rate constant, k (min^{-1})	Correlation coefficient, R^2
S2	16.3×10^{-3}	0.987
S3	9.20×10^{-3}	0.986
S4	4.70×10^{-3}	0.978
S5	4.10×10^{-3}	0.975
S6	3.00×10^{-3}	0.991
S8	3.20×10^{-3}	0.977
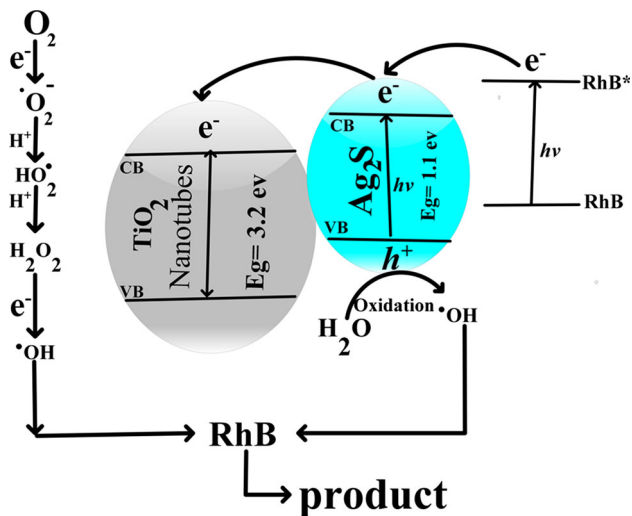
Fig. 8 Mechanism of photo catalytic degradation of rhodamine B using Ag$_2$S/NTs nanocomposites as the catalyst

band of TiO$_2$, whereas the photo-induced holes still remained in the VB of Ag$_2$S. As a result of this, there is less recombination of electrons and holes [Reaction (12)]. Such an interfacial charge transfer will bring down recombination of photo-generated charge carries. Therefore the above results we presume the hetero-structures do larger the ab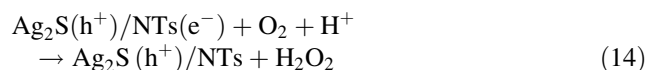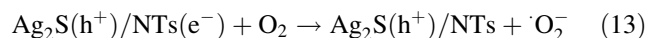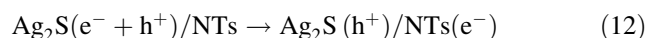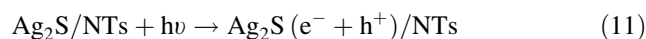sorption range to visible-light region. The photo-generated electrons on irradiated Ag$_2$S react with the surface adsorbed O$_2$ molecules to yield superoxide radical anion (O$_2^-$) [Reaction (13)] and hydrogen peroxide (H$_2$O$_2$) [Reaction (14)]. Elmolla et al. [35] reported that the H$_2$O$_2$ is considered to have two functions in the photo catalytic process. It accepts a photo-generated electron from the conduction band of the semiconductor to form $^{.}$OH and OH$^-$ radicals [Reaction (15)]. In addition, it forms $^{.}$OH and $^-$OH radicals according to the reaction (16). Then, dye molecules are oxidized by these oxidants step by step [Reaction (17)]. In addition, the holes themselves can directly oxidize dye molecules (Rh B), and this is considered as the dominant pathway, because it is the prerequisite step for the photo catalytic reaction that dye molecules adsorbed on the surface of Ag$_2$S/NTs [Reaction (18)] [34]. In this study, it is thought that both indirect oxidation by

hydroxyl radical and direct oxidation by holes simultaneously functioned to oxidize dye molecules. By this token, the combination of Ag$_2$S contributes to enhance photo catalytic efficiency under visible light irradiation owing to the photo-induced interfacial charge transfer. On irradiation light, photo-oxidation of rhodamine B takes place leading to the formation of RhB radial cation. In this pathway, the degradation occurs by de-ethylation of RhB radial cation because of attack by one of the active oxygen species (HO$_2^-$, O$_2^-$ or $^{.}$OH) on the N-ethyl group leading to the formation of de-ethylated intermediates (N,N,N$'$-tri-ethylated rhodamine, N,N$'$-di-ethylated rhodamine, N-ethylated rhodamine and rhodamine) with different absorption maxima. There is another pathway that including the degradation of rhodamine B chromophore because of attack by hydroxyl radicals on its chromophoric structure. Destruction of conjugated chromophore structure leads to the formation of intermediates (organic acids and various alcohols) and finally to CO$_2$ and H$_2$O [22, 36–38].

$$Ag_2S/NTs + h\upsilon \rightarrow Ag_2S\,(e^- + h^+)/NTs \qquad (11)$$

$$Ag_2S(e^- + h^+)/NTs \rightarrow Ag_2S\,(h^+)/NTs(e^-) \qquad (12)$$

$$Ag_2S(h^+)/NTs(e^-) + O_2 \rightarrow Ag_2S(h^+)/NTs + \,^{.}O_2^- \quad (13)$$

$$\begin{aligned} &Ag_2S(h^+)/NTs(e^-) + O_2 + H^+ \\ &\quad \rightarrow Ag_2S\,(h^+)/NTs + H_2O_2 \end{aligned} \qquad (14)$$

$$\begin{aligned} &Ag_2S(h^+)/NTs(e^-) + H_2O_2 \rightarrow Ag_2S\,(h^+)/NTs + \,^{.}OH \\ &\quad\quad\quad\quad\quad\quad\quad\quad\quad\quad\quad\quad\quad + OH^- \end{aligned}$$
$$(15)$$

$$H_2O_2 + \,^{.}O_2^- \rightarrow \,^{.}OH + OH^- + O_2 \qquad (16)$$

$$Dye\,(RhB) + \,^{.}O_2^-\,(H_2O_2/\,^{.}OH) \rightarrow Products \qquad (17)$$

$$\begin{aligned} Ag_2S(h^+)/NTs + Dye_{ads} &\rightarrow Ag_2S/NTs + Dye_{ads}^{.+} \\ &\rightarrow Ag_2S/NTs + Products \end{aligned} \quad (18)$$
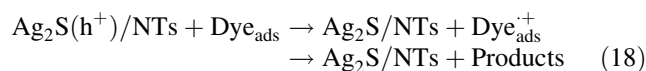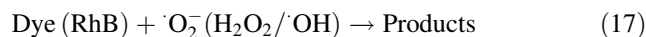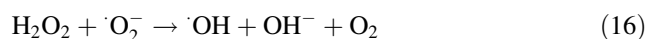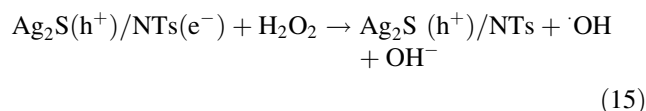
4 Conclusion

In summary, a simple method for the synthesis of Ag$_2$S/NTs nanocomposites has been described. The nanocomposites were characterized using different analytical

techniques. Characterization of Ag$_2$S/NTs samples indicated that the number of SILAR cycles significantly influenced the morphology and photo catalytic activity of fabricated films. The degradation of rhodamine B was used as a model reaction to evaluate the photo catalytic activity of the obtained samples. Compared to bare NTs, the Ag$_2$S/NTs nanocomposite samples exhibited an enhancement in apparent rate constant. The better photo activity of these samples can be assigned to the enhanced visible absorption by Ag$_2$S. The recyclability of prepared samples showed that these samples have high stability. Compared with nanoparticles, nanotubes arrays not only have three-dimensional tubular structure and large specific surface area, but also can be used repeatedly and conveniently. These new nanocomposite catalysts may have potential application as a good photo catalyst in a scale-up for industrial water remediation.

References

1. J. Fenoll, P. Hellín, P. Flores, C.M. Martínez, S. Navarro, Chemosphere **87**, 954 (2012)
2. Y. Li, Y. Wang, J. Kong, H. Jia, Z. Wang, Appl. Surf. Sci. **344**, 176 (2015)
3. T.M. Wang, H.Y. Wang, P. Xu, X.C. Zhao, Y.L. Liu, S. Chao, Thin Solid Films **334**, 103 (1998)
4. J. Zhang, W. Chen, J. Xi, Z. Ji, Mater. Lett. **79**, 259 (2012)
5. M.M. Momeni, Appl. Phys. A **119**, 1413 (2015)
6. Y.C. Li, Q. Ma, J. Han, L.L. Ji, J.X. Wang, J.Y. Chen, Y.Q. Wang, Appl. Surf. Sci. **297**, 103 (2014)
7. M.M. Momeni, Y. Ghayeb, J. Alloys Compd. **637**, 393 (2015)
8. M.M. Momeni, Appl. Surf. Sci. **357**, 160 (2015)
9. W. Shu, Y.L. Liu, Z.Y. Peng, K.Q. Chen, C. Zhang, W. Chen, J. Alloy Compd. **563**, 229 (2013)
10. M.M. Momeni, Y. Ghayeb, J. Iran. Chem. Soc. **13**, 481 (2016)
11. R. Sugranez, J.I. Álvarez, M. Cruz-Yusta, I. Mármol, J. Morales, J. Vila, L. Sánchez, Build. Environ. **69**, 55 (2013)
12. M.M. Momeni, Y. Ghayeb, J. Mater. Sci. Mater. Electron. **27**, 1062 (2016)
13. M.M. Momeni, Y. Ghayeb, Ceram. Int. **42**, 7014 (2016)
14. E.A. Kozlova, N.S. Kozhevnikova, S.V. Cherepanova, T.P. Lyubina, EYu. Gerasimov, V.V. Kaichev, A.V. Vorontsov, S.V. Tsybulya, A.A. Rempel, V.N. Parmon, J. Photochem. Photobiol. A **250**, 103 (2012)
15. Y. Hassan, C.H. Chuang, Y. Kobayashi, N. Coombs, S. Gorantla, G.A. Botton, M.A. Winnik, C. Burda, G.D. Scholes, J. Phys. Chem. C **118**, 3347 (2014)
16. S.B. Bubenhofer, C.M. Schumacher, F.M. Koehler, N.A. Luechinger, R.N. Grass, W.J. Stark, J. Phys. Chem. C **116**, 16264 (2012)
17. K.P. Acharya, T.R. Alabi, N. Schmall, N.N. Hewa-Kasakarage, M. Kirsanova, A. Nemchinov, E. Khon, M. Zamkov, J. Phys. Chem. C **113**, 19531 (2009)
18. M. Gholami, M. Qorbani, O. Moradlou, N. Naseri, A.Z. Moshfegh, RSC Adv. **4**, 7838 (2014)
19. H. Kisch, Angew. Chem. Int. Ed. **52**, 812 (2013)
20. A. Tubtimtae, K.L. Wu, H.Y. Tung, M.W. Lee, G.J. Wang, Electrochem. Commun. **12**, 1158 (2010)
21. B. Liu, D. Wang, Y. Zhang, H. Fan, Y. Lin, T. Jiang, T. Xie, Dalton Trans. **42**, 2232 (2013)
22. Y. Du, B. Xu, T. Fu, M. Cai, F. Li, Y. Zhang, Q. Wang, J. Am. Chem. Soc. **132**, 1470 (2010)
23. M.C. Neves, J.M.F. Nogueira, T. Trindade, M.H. Mendonca, M.I. Pereirac, O.C. Monteiro, J. Photochem. Photobiol. A Chem **204**, 168 (2009)
24. I. Grozdanov, Appl. Surf. Sci. **84**, 325 (1995)
25. M.C. Neves, O.C. Monteiro, R. Hempelmann, A.M.S. Silva, T. Trindade, Eur. J. Inorg. Chem. **28**, 4380 (2008)
26. Y. Xie, S.H. Heo, Y.N. Kim, S.H. Yoo, S.O. Cho, Nanotechnology **21**, 015703 (2010)
27. M. Hosseini, M.M. Momeni, M. Faraji, Electroanalysis **23**, 1654 (2011)
28. Y.F. Nicolau, Appl. Surf. Sci. **23**, 1061 (1985)
29. P. Ma, H. Yu, W. Wang, H. Wang, J. Zhang, Z. Fu, Phys. Chem. Chem. Phys. **18**, 3638 (2016)
30. W. Yang, T. Xie, D. Wang, Colloids Surf. A Physicochem. Eng. Asp. **433**, 25 (2013)
31. M.M. Momeni, Z. Nazari, Ceram. Int. **42**, 8691 (2016)
32. M.M. Momeni, Y. Ghayeb, J. Mol. Catal. A Chem. **417**, 107 (2016)
33. M.M. Momeni, Y. Ghayeb, J. Mater. Sci. Mater. Electron. **27**, 3318 (2016)
34. L. Yu, D. Wang, D. Ye, Sep. Purif. Technol. **156**, 708 (2015)
35. E.S. Elmolla, M. Chaudhuri, Desalination **252**, 46 (2010)
36. L. Zhu, Z.D. Meng, W.C. Oh, J. Nanomater. **2012**, 1 (2012)
37. T. Wu, T. Liu, J. Zhao, J. Phys. Chem. B **102**, 5845 (1998)
38. C. Chen, W. Zhao, J. Li, J. Zhao, Environ. Sci. Technol. **36**, 3604 (2002)